Dynamics and thermodynamics of fragment emission from excited sources

M. J. Ison and C. O. Dorso
Departamento de Física, Facultad de Ciencias Exactas y Naturales, Universidad de Buenos Aires, Pabellón I, Ciudad Universitaria, Nuñez, 1428, Buenos Aires, Argentina
(Received 17 December 2004; published 22 June 2005)

In this paper we study the process of fragmentation of highly excited Lennard-Jones drops by studying the emission of stable fragments (clusters recognizable in configuration space that live more than a minimum lifetime). We focus on the dynamics and thermodynamics of the emitting sources and show, among other things, that this kind of process is a mixture of sequential and simultaneous events and that simultaneous events have a broad time distribution. We also show how a local equilibrium scenario comes up on top of expanding collective motion, allowing us to define and explore a local temperature, which turns out to be a strongly time-dependent quantity, signaling that we are facing an out-of-equilibrium process.

DOI: 10.1103/PhysRevC.71.064603 PACS number(s): 25.70.Mn, 25.70.Pq, 02.70.Ns

I. INTRODUCTION

The problem of fragmentation attracts the interest of physicists in many branches of physics. In particular, in the field of metallic clusters and nuclear collisions, one deals with systems that are both finite and nonextensive. In these cases, the size of the system under analysis is near the range of the interaction potential and calls for a careful analysis.

This problem has been analyzed from different points of view, and we classify them in two main groups, i.e., statistical models and dynamical models. In the first case [1–3] the main assumption is that the fragmentation process is driven by phase-space occupancies. The ever-present assumption of *freeze-out* volume states that the system fragments in an equilibrium scenario at a given fixed volume and that thermal and/or chemical equilibrium is reached, in correspondence with the description chosen by the researcher (i.e., micro-canonical, canonical, or grand canonical). This kind of analysis has also been performed in systems that have *a priori* little relation with the nuclear problem, as for instance, the lattice gas model [4] and the Ising model [5]. The motivation for the use of these kinds of systems is that they display true phase transitions that are supposed to take place in nuclear systems in the multifragmentation regime.

Recently, statistical models have been extended to the isobaric isothermal ensemble [6]. Even in this kind of formulation, there have been efforts to include nonequilibrium effects like, for example, the presence of expansive collective motion [4].

Dynamical models include, among others, classical [7–10] and quantum [11,12] types, which are fully microscopic. This category also includes those based on numerical realization of kinetic equations such as the Boltzmann-Uehling-Uhlenback, and the VLD. Focusing on the fully microscopic models, their main advantage is that we can analyze correlations of all orders at all times. Moreover, nonequilibrium features of the process can be readily explored.

In what follows, we will focus on the analysis of small Lennard-Jones (LJ) drops, i.e., a system in which the dynamics is generated by a Hamiltonian with a very short-range strong repulsion and a short-range attraction. In this way, we retain the main characteristics of the nuclear interaction force. On the other hand, all quantum properties are disregarded. Quantum features like the Pauli exclusion principle, wave dynamics, or shell effects are expected to play a stronger role in the later stage of the evolution and cooling of the excited fragments than in the early highly collisional stage of the reaction; therefore, our approach gives the general classical framework which should help in understanding the true nuclear behavior.

Continuing with a series of previous works, we will study the dynamics of highly excited 147-particle LJ drops [8,13] (and references therein). Previously, we mainly considered the problem of fragment formation. We have shown that this phenomenon takes place in phase space, and as such it is not an experimental observable. Only emitted fragments can be detected experimentally, i.e., when they are well defined in configuration space. In this report, we will focus our attention on the properties of the emitting sources and the corresponding emitted fragments. At this point, it is worthwhile to define what we understand as emission. We say that a fragment has been emitted when it is recognizable in configuration space. We have already made this classification [14] and have shown that there are well-defined time scales for the processes of fragment formation and fragment emission.

There are many unsolved questions regarding the fragmentation process. One of the main ones is the proper characterization of the degree of equilibration of the fragmenting system. If system equilibration and fragmentation are driven by phase-space accessibility, no traces of collective expanding motion should be present (no Coulomb force is present in our calculations, and collective motion can only be generated by interparticle collisions). Moreover, this equilibrated state should be detectable in our simulations. In fact, we will show that no evidence of such behavior emerges from our calculations.

This equilibrium problem is also related to the sequential vs simultaneous pictures. To explore this effect we will define a proper time scale. The numerical simulations are performed in such a way that coordinates and momenta are recorded every one-fifth of the natural period (one-fifth of the inverse of

Einstein's frequency), and then we will define as simultaneous all events that take place within one natural period. In this way, we will show that both simultaneous and sequential fragmentations coexist at all energies.

Because of this mixture of sequential and simultaneous fragmentation, it is relevant to study the dynamical and thermodynamical evolution of the biggest source. In particular, we will use the concept of effective temperature, as is usually done in fragmentation studies. We will about effective temperature because there is no such thing as a heat bath, but there is evidence [14] that some degree of local equilibration is attained by the system, in particular at the time of fragment formation. In fact, our effective temperature will be related to the intrinsic (chaotic) kinetic energy, i.e., what remains from the total kinetic energy once the part related to collective degrees of freedom is removed. In this way, we will show that the biggest source cools down as it expands and emits fragments.

Finally, we will show that the reducibility effect (i.e., the possibility of describing the fragmentation process as a sequence of independent fragment emission events) arises naturally in the present context.

This paper is organized as follows: In Sec. II, we review the different fragment recognition algorithms currently in use. In Sec. III, we present different temperature definitions relevant to the analysis of the evolution of the excited drops. Section IV deals with the model we study. Section V includes all the results we have obtained in our numerical simulations (fragment mass distributions, characteristic times, temperature of the emitting sources, role of the radial flux, etc.). Finally, conclusions will be drawn.

II. FRAGMENT RECOGNITION ALGORITHMS

The problem of analyzing molecular dynamics calculations is an old one and is not completely settled. To our knowledge, there are three main fragment recognition algorithms in use: MST, MSTE, and ECRA.

The simplest and more intuitive cluster definition is based on correlations in configuration space: particle i belongs to cluster C if there is another particle j that belongs to C and $|\mathbf{r_i} - \mathbf{r_j}| \leqslant r_{\rm cl}$, where $r_{\rm cl}$ is the clusterization radius. If the interaction potential has a cutoff radius $r_{\rm cut}$, then $r_{\rm cl}$ must be equal or smaller than $r_{\rm cut}$; in this work, we chose $r_{\rm cl} = r_{\rm cut} = 3\sigma$. The algorithm that recognizes these clusters is known as the minimum spanning tree (MST). The main drawbacks of this method is that only correlations in $\mathbf{q}$ space are used, neglecting completely the effect of momentum.

An extension of the MST is the minimum spanning tree in energy space (MSTE) algorithm [15]. In this case, a given set of particles $i, j, \ldots, k$ belongs to the same cluster C_i if

$$\forall i \epsilon C_i, \qquad \exists j \epsilon C_i / e_{ij} \leqslant 01, \tag{1}$$

where $e_{ij} = V(r_{ij}) + (\mathbf{p}_i - \mathbf{p}_j)^2/2\mu$, and μ is the reduced mass of the pair $\{i, j\}$. MSTE searches for configurational correlations between particles considering the relative momenta of particle pairs. In spite of not being supported by a physically sound definition of a cluster, the MSTE algorithm typically recognizes fragments earlier than MST. Furthermore, because of its sensitivity to recognizing promptly emitted particles, it can be useful for studying the preequilibrium energy distribution of the participant particles.

A more robust algorithm is based on the most-bound partition (MBP) of the system [16]. The MBP is the set of clusters $\{C_i\}$ for which the sum of the fragment internal energies attains its minimum value, that is,

$$\begin{aligned} \{C_i\} &= \underset{\{C_i\}}{\operatorname{argmin}} \left[E_{\{C_i\}} = \sum_i E_{\rm int}^{C_i} \right] \\ E_{\rm int}^{C_i} &= \sum_i \left[\sum_{j \in C_i} K_j^{\rm c.m.} + \sum_{\substack{j,k \in C_i \\ j \leqslant k}} V_{j,k} \right], \end{aligned} \tag{2}$$

where the first sum in (3) is over the clusters of the partition, $K_j^{\rm c.m.}$ is the kinetic energy of particle j measured in the center of mass frame of the cluster that contains particle j, and V_{ij} stands for the interparticle potential. It can be shown that clusters belonging to the MBP are related to the mostbound density fluctuation in **r-p** space [16].

The algorithm that finds the MBP is known as the early cluster recognition algorithm (ECRA). Since ECRA searches for the most-bound density fluctuations in **q-p** space, valuable space and velocity correlations can be extracted at all times especially at the very early stages of the evolution. This has been used extensively in many fragmentation studies [7,8,16, 17] and has helped in discovering that fragments are formed very early in the evolution.

When we use the three above-mentioned algorithms and we apply a criterion based on the average microscopic stability of the clusters (see, for example [7]) to determine the corresponding times of fragment formation, three time scales emerge, which satisfy the following relation: $\tau_{\rm ECRA} < \tau_{\rm MSTE} < \tau_{\rm MST}$. But the meaning of each of these times is quite different. $\tau_{\rm ECRA}$ refers to that time at which, on average, clusters attain microscopic stability regardless of the structure of the system in q space. $\tau_{\rm MSTE}$ has a rather obscure meaning because the MSTE algorithm is not well defined from the physical point of view for dynamical problems. Finally $\tau_{\rm MST}$ refers to that time at which, on average, microscopic stability is attained for free fragments. Please take into account that depending on the definition of $r_{\rm cl}$ this last condition can be rephrased as "weakly interacting fragments."

III. TEMPERATURES

Because we are aiming to perform some kind of thermodynamic analysis of the system, a prescription for the calculation of the temperature in small (and probably out of equilibrium) systems is to be given. It might be proper to remind the reader that in our case, and also in nuclear experiments, systems expand and fragment in a vacuum; i.e., there is no external heat bath or external pressure. Therefore, our definitions of temperature stand for an "effective kinetic temperature" and are not to be confused with the usual thermodynamic definition of temperature. On the other hand, we will frequently make

use of the concept of local temperature, which is accepted in modern thermodynamical theory [18]. We should also keep in mind that we are going to analyze physical processes in the framework of the molecular dynamics ensemble, which is the microcanonical ensemble plus the conservation of total linear and angular momentum. Let us assume that at a given stage of the evolution of the system we can identify the biggest fragment according to the MST algorithm.

To study the time evolution of the thermodynamics of the biggest emitting source, we define the local temperature $T_{\rm loc}(t)$ as the velocity fluctuations around the mean radial expansion of the biggest source. So, we first introduce the mean radial velocity of the biggest source,

$$v_{\rm rad}(t) = \left\langle \frac{1}{N_{\rm BF}} \sum_{i=1}^{N_{\rm BF}} \frac{\mathbf{v}_i(t)\cdot\mathbf{r}_i(t)}{|\mathbf{r}_i(t)|} \right\rangle_e , \tag{3}$$

Where $N_{\rm BF}$ indicates the number of particles of the biggest source at time t, and $\langle\,\rangle_e$ denotes an average over all events. Both $\mathbf{v}_i(t)$ and $\mathbf{r}_i(t)$ are measured from the center of mass of the biggest source. Taking into account that collective motion should not be considered to calculate the temperature, we define the local temperature $T_{\rm loc}$ as

$$T_{\rm loc}(t) = \frac{2}{3N_{\rm BF}} \sum_{i=1}^{N_{\rm BF}} \frac{m}{2} [\mathbf{v}_i(t) - v_{\rm rad}(t)\cdot\hat{\mathbf{r}}_i(t)]^2. \tag{4}$$

This definition is closely related to the one used in [7] for the analysis of expanding systems. In that case, we obtained the local temperature of the system by the following procedure. We divided our drops in concentric spherical regions, centered in the c.m. of the system, of width $\delta r = 2\sigma$. The mean radial velocity of region i in this case is

$$v^{(i)}_{\rm radshell}(t) = \frac{1}{N_i(t)} \sum_{\rm ev} \sum_{j\in i} \frac{\mathbf{v}_j(t)\cdot\mathbf{r}_j(t)}{|\mathbf{r}_j(t)|}, \tag{5}$$

where the first sum runs over the different events for a given energy, the second over the particles j that belong, at time t, to region i; $\mathbf{v}_j$ and $\mathbf{r}_j$ are the velocity and position of particle j. $N_i(t)$ is total number of particles belonging to region i in all the events. Then the local temperature, which will be called $T^{(i)}_{\rm shell}$, is defined as

$$T^{(i)}_{\rm shell} = \frac{2}{3}\frac{1}{N_i} \sum_{j\in i} \frac{1}{2} m \left(\mathbf{v}_j - \frac{v^{(i)}_{\rm rad}\cdot\mathbf{r}_j}{|\mathbf{r}_j|} \right)^2 , \tag{6}$$

where N_i is the total number of particles in cell i in all events.

The validity of Eqs. (4) and (6) relies on the *conjecture* that the fragmenting system achieves local equilibrium (local equilibrium hypothesis). Whereas in the last case all particles in the inner shells should be equilibrated, the advantage of dealing with the local temperature (4) relies on the fact that only the biggest source is assumed to have reached some degree of equilibration. In this paper, we will focus mainly on this definition. If the biggest source is assumed to have reached equilibrium, the velocity distribution should be

$$f(v) = \rho \left(\frac{m\beta}{2\pi} \right)^{3/2} e^{-\beta\frac{m}{2}(v-v_{\rm rad})^2}. \tag{7}$$

A first approach on the study of the local equilibrium hypothesis (LEH) consists in analyzing the isotropy of the velocity fluctuations around the expansion. For this purpose, we introduce the radial and transversal local temperatures

$$T^{\rm rad}_{\rm loc} = \frac{2}{N_{\rm BF}} \sum_{i=1}^{N_{\rm BF}} \frac{m}{2} \{[(\mathbf{v}_i(t) - v_{\rm rad}(t)\cdot\hat{\mathbf{r}}_i(t)]\cdot\hat{\mathbf{r}}_i(t)\}^2, \tag{8}$$

$$T^{\rm tra}_{\rm loc} = \frac{2}{N_{\rm BF}} \sum_{i=1}^{N_{\rm BF}} \frac{m}{2} \{[(\mathbf{v}_i(t) - v_{\rm rad}(t)\cdot\hat{\mathbf{r}}_i(t)]\cdot\hat{\mathbf{r}^{\perp}}_i(t)\}^2. \tag{9}$$

A more profound analysis of the accuracy of the LEH is the study of the velocity distribution function and its comparison with (7). For this purpose, we fit the velocity distribution resulting from our numerical simulations with the formula (7) and then we calculate the significance S of this fit.

To address the question of whether both distributions are different, we will perform a Pearson χ^2 test [19]. If the significance is high enough not to reject the hypothesis that both distributions are different, we obtain as a byproduct that the effective kinetic temperature can be calculated as

$$T_{\rm max} = m\sigma^2, \tag{10}$$

where σ is the width of the velocity distribution.

IV. THE MODEL

The system under study is composed, as in previous works, of $N = 147$ particles interacting via a truncated and shifted Lennard-Jones potential, with a cutoff radius $r_{\rm cut} = 3\sigma$. Energies are measured in units of the potential well (ϵ), and the distance at which the LJ potential changes sign (σ), respectively. The unit of time used is $t_0 = \sqrt{\sigma^2 m/48\epsilon}$.

The typical frequency of such potential is $\nu_0 \sim \frac{1}{5t_0}$. This defines a minimum time scale for the stability of an interacting system.

The equations of motion were integrated using the velocity Verlet algorithm, which preserves volume in phase space. We used an integration time step of $0.01t_0$ and performed a microcanonical sampling every $1t_0$ up to a final time of $t = 250t_0$. This time scale was chosen because is has proven to be long enough to allow the system to attain microscopic stability.

As stated in the previous section, we are mainly interested in the properties of fragments in configuration space. Then we are to analyze the MD evolutions using the MST algorithm. We define a fragmentation process when a source emits a *s*table fragment of at least four particles, i.e., the MST determination of fragments is complemented with a temporal stability condition, the emitted particles must remain together for at least $5t_0$ to be considered an emitted fragment. Otherwise, if the particles fly apart within $5t_0$ we will consider it to be an evaporation process.

The evolutions are analyzed in an event-by-event basis, and the times at which fragmentation takes place are determined.

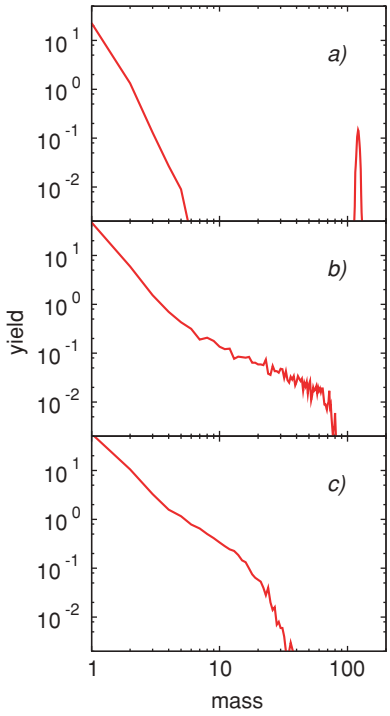

FIG. 1. (Color online) Asymptotic mass spectra. Energies $E = -2.0\epsilon$, 0.0ϵ, and 2.0ϵ are displayed in (a), (b), and (c), respectively.

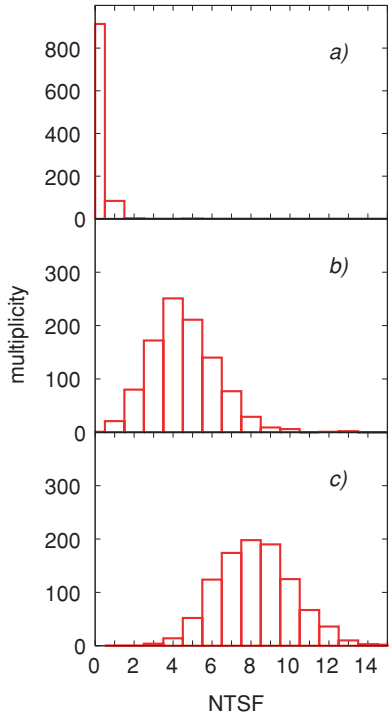

FIG. 2. (Color online) Distribution of NTSF for $E = -2.0\epsilon$, 0.0ϵ, and 2.0ϵ are shown in (a), (b), and (c), respectively.

V. NUMERICAL EXPERIMENTS

Initial configurations are built as dense drops in q space (region C of the phase diagram of a finite LJ system, see [20]). The total linear and angular momentum of the drops are removed, and then velocities are scaled with a Maxwellian distribution so that the system has the desired value of total energy.

We covered a broad range of energies, namely, -2.0ϵ, -1.0ϵ, -0.5ϵ, -0.2ϵ, 0.0ϵ, 0.2ϵ, 0.5ϵ, 1.0ϵ, and 2.0ϵ (all reported energies are per particle). For each energy, 1000 events were calculated.

A. Fragment mass distributions

The range of energies we used covers all regions of interest in multifragmentation. In Fig. 1, it can be clearly seen that the asymptotic mass distributions go from U-shaped, at low energies, to exponentially decaying ones, at high energies. Between these shapes a power-law (panel b) in Fig. 1 can be found. Technical details of the fitting procedure used to identify these mass spectra as a power law are given elsewhere [21], but we would like to point out that the fitting procedure excludes the biggest fragment at each event, and also explicitly excludes monomers, dimers, and trimers.

We have studied the distribution of the number of times the system fragments (NTSF) for all events as a function of the energy of the system. In this case, our approach is to follow the dynamics of the biggest source. At a given time $t_i = nt_0$, we identify the biggest MST fragment and check for the particles that belonged to this fragment at t_i and formed a smaller cluster at $t = (n + 5)t_0$. We have chosen $5t_0$ as our threshold to accept the cluster as stable because that is of the order of the inverse of the natural frequency. In this way, we show in Fig. 2 this distribution for energies per particle $E = -2.0\epsilon$, 0.0ϵ, and 2.0ϵ. It can be easily seen that, in this range of energy, as the energy of the system is increased, the maximum of the multiplicity distribution shifts toward higher values while the width of the distribution increases.

B. Characteristic times

The characterization of the fragmentation process as sequential or simultaneous is a matter of debate. In our calculation, the analysis of these kinds of things is straightforward once the proper time scales are defined. The dynamics of our system is driven by the LJ interaction potential. This potential has a natural period (inverse of the Einstein frequency) of $5t_0$, with t_0 defined above. According to this, as stated above, particles will be considered as a cluster if they remain together for at least one period. We then define as simultaneous all emissions, i.e. all fragments that can be recognized as emitted, during a period of $5t_0$ and remain together at least for that period of time.

There are different characteristic times that can be explored. First, we will look at the first and last time of emission. This means that we record for each of our evolutions the time at which the first fragmentation takes place according to our definition of an emission process. The results of that calculation are displayed in Fig. 3.

We can see that at high energies ($E = 2.0\epsilon$), the distribution of times is narrower than at lower energies and does not seem

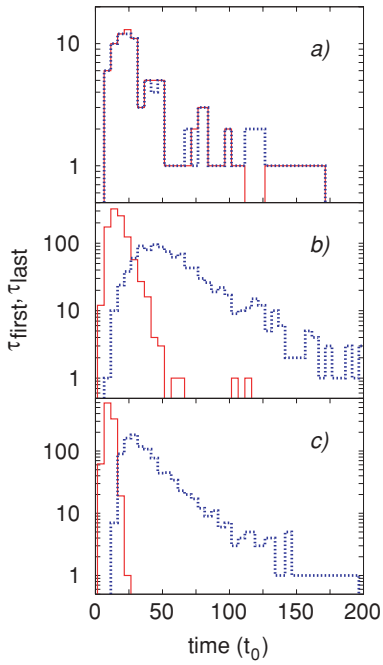

FIG. 3. (Color online) Distribution of first (full line) and last (dotted line) time of emission. Energies: $E = -2.0\epsilon$, 0.0ϵ, and 2.0ϵ are displayed in panels (a), (b), and (c), respectively.

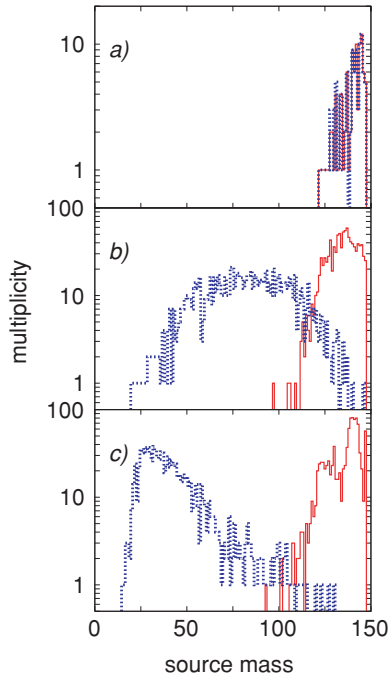

FIG. 5. (Color online) Same as Fig. 3, but for mass of the emitting sources for the first (full line) and last (dotted line) emissions.

to fit the view of a simultaneous process in configuration space. (This issue will be further analyzed in Sec. V G). Another view of the same data is shown in Fig. 4 in which what we show is the corresponding lapse of time between the first and last emission for each event. Once again, the distribution gets broader as the energy gets lower (the comparison should be restricted to events corresponding to $E = 0.0\epsilon$ and 2.0ϵ because of the very few emission processes found at $E = -2.0\epsilon$. To further illustrate the kind of process we are facing, we show in Fig. 5 the distribution of the mass of the emitting sources for the times of first and last emissions.

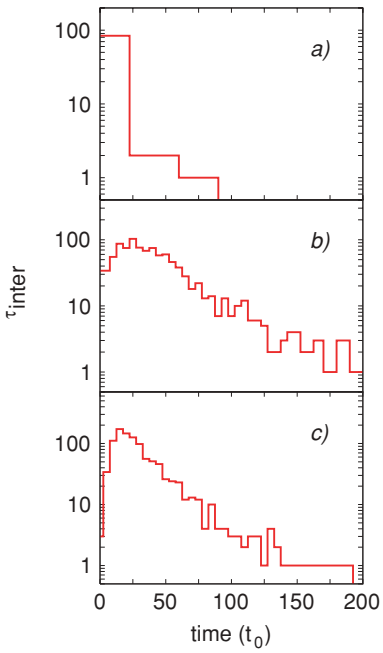

FIG. 4. (Color online) Same as Fig. 3, but for lapse of time between the first and last emissions.

The most relevant result of this figure is the presence, in panel (b), of a broad range of masses at which the last emission takes place, which is to be expected since the value of energy ($E = 0.0\epsilon$) corresponds to a power-law mass distribution.

The reason why we stated above that these results do not seem to fit the simultaneous emission picture without ensuring it is because we can also explore the possibility of the occurrence of massive emission events (when a rather large portion of the mass of the biggest is emitted within $5t_0$). Even though emission events can be found in a rather large scale of time, one may wonder if massive emission events have a definite characteristic time which would sustain the simultaneous picture.

We have used two definitions of massive emission event (MEE). The first considers a MEE if the mass of the emitted fragment is at least 30% of the total mass of the biggest source at the time of emission. The second states that a MEE has taken place if the mass of the biggest emitted fragment is at least composed of 40 particles.

The results of such calculations are shown in Fig. 6. It is immediately seen that massive emission, according to definition 1, can take place at any time during the evolution; whereas under the second definition (which is more restrictive), almost no massive events occur for times greater than $t \sim 100t_0$. Also notice that the lower value of energy we used ($E = -2.0\epsilon$) is not present because no massive fragmentations were found.

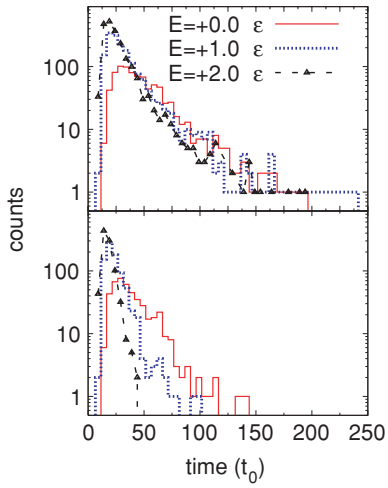

FIG. 6. (Color online) Distribution of emission times of massive fragments using definition 1 (top) and definition 2 (bottom); see text for details.

When gathering all these results together, we conclude that for the energies displayed in these figures, the process can be viewed as a mixture of sequential and simultaneous breakup.

C. Temperatures of the emitting sources

It is natural to think that as the sources emit fragments they will undergo a cooling process. We should keep in mind that we are trying to analyze things in an event-by-event basis, without performing averages that would obscure the picture. To gain knowledge of the microscopic view of the fragmentation phenomena, we calculated the evolution of the temperature, for a given energy and for each time step in which a fragmentation event takes place. The temperature is that of the emitting source in the time step prior to the time step in which the emission takes place. We then plot all this information in a single graph (see Fig. 7).

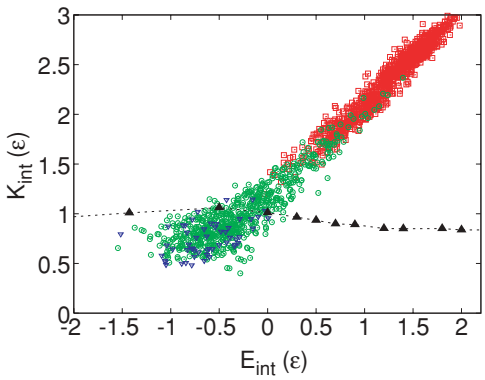

FIG. 7. (Color online) Internal kinetic energy of the emitting source as a function of its total internal energy for three NTSFs. Empty (red) squares denote the 1st emission process. Empty (green) circles denote the 8th emission process, and empty (blue) triangles indicate the 12th emission process. Full (black) triangles stand for the caloric curve of the expanding system.

In Fig. 7, we show the result for the analysis of 1000 events at an initial energy of $E = 2.0\epsilon$. To make the figure more readable, we are only showing the above-described temperature for the first, last, and maximum multiplicity fragmentation events. It is clearly seen that the internal kinetic energy is linear with the total internal energy and displays a cooling behavior. This overall behavior will not change if we consider not only fragmentation events but also evaporation events. It is interesting to note that if one were to calculate temperatures from the analysis of the emitted light fragments (monomers, dimers, and trimers), one would be sampling a source that starting from a rather high temperature cools down monotonically. So the corresponding temperature should display a maximum at early times and decrease later [22]. This is not a problem at all because the system is out of equilibrium, and therefore the kind of measurements we are referring to at this point do not correspond to stable systems. What might be improper is to talk about temperature instead of "effective temperature." A more quantitative calculation is under development and will be communicated shortly.

D. The role of radial flux

In a series of previous works [9], we showed that if the presence of collective (nonthermal) motion is not taken into account, one obtains a wrong result: the presence of a vapor branch in to the caloric curve. Only when the radial flux is properly incorporated into the definition of the temperature does one find that the nonequilibrium process of multifragmentation appears as an almost constant temperature region at high energies. In particular, in paper [14] we calculated the time of fragment formation of this system (using the ECRA phase-space method). The values of the mean radial velocity calculated for the biggest source in each event according to Eq. (3) are shown in Fig. 8.

In Fig. 9 we show the local temperature of the biggest source at time of fragment formation, as a function of the total energy (full line). The dotted line is included to emphasize the effect of not removing the radial collective motion when calculating caloric curves. As explained in Sec. III, temperatures were calculated from velocity fluctuations around the collective motion.

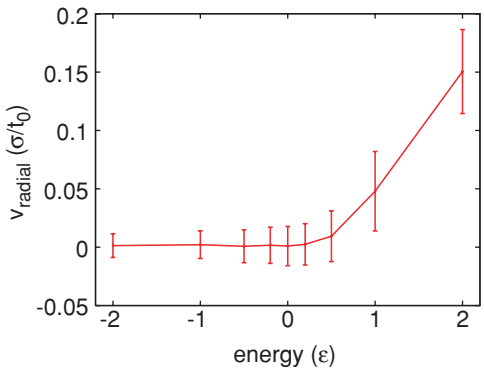

FIG. 8. (Color online) Radial flux as a function of energy at the time of fragment formation $\tau_{\rm ff}$.

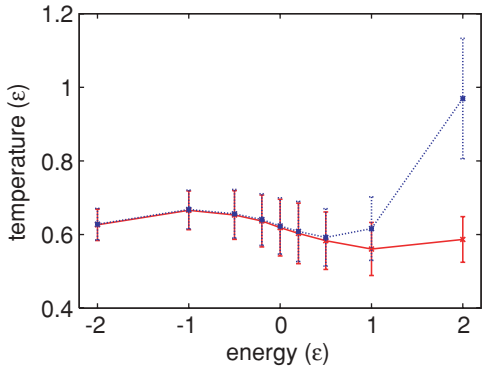

FIG. 9. (Color online) Local temperature of the biggest source at $\tau_{\rm ff}$ (straight red line) and "fake temperature" (dotted blue line). The fake temperature is calculated from the total kinetic energy of the biggest source without taking into account the importance of the radial flux.

To see how the picture emerging from a phase-space analysis relates to the main topic of this paper, i.e., the analysis in configuration space, we calculated the temperature of the emitting sources at the stage of evolution that corresponds to the maximum of the multiplicity distribution [for example, looking at Fig. 2(b), the maximum of the distribution turns out to be NTSF = 4)]. From this kind of analysis, we get the empty circles of Fig. 10. It can be easily seen that both approaches give the same temperature.

E. Local equilibrium hypothesis (LEH)

To check the hypothesis of local equilibrium, which we used in previous sections, we performed the following calculation. Because in a local equilibrium scenario the fluctuations of velocity should be the same for the radial and transversal directions, we evaluated Eqs. (8) and (9) for a single event at the three energies chosen as examples in this work. In each of the three panels of Fig. 11, each of which corresponds to a different total energy (see caption for details), we show our

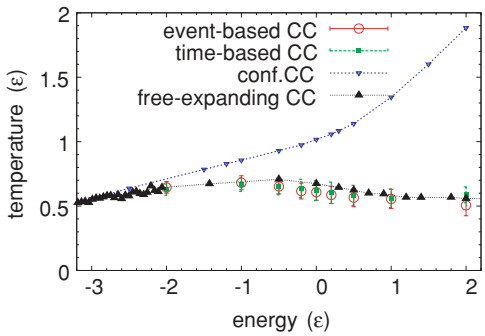

FIG. 10. (Color online) Comparison of caloric curves obtained by different thermometers. Empty circles correspond to an event-based temperature. Filled squares correspond to the temperature of the biggest source at time of frament formation. Upward triangles denote the local temperature ($T_{\rm shells}$), and the dotted line with downward triangles corresponds to the caloric curve obtained for a constrained system with density $\rho = 0.17\sigma^{-3}$.

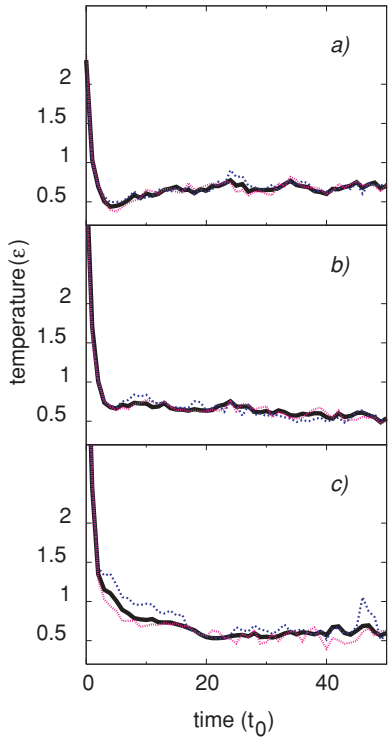

FIG. 11. (Color online) Radial (dotted line), transversal (thin line), and local (full line) temperatures of the biggest source for $E = -2.0\epsilon$ (a), 0.0ϵ (b), and 2.0ϵ (c).

three definitions of temperature. It is immediately seen that all of them are essentially the same, except in the very early stages of the evolution (when times are much shorter than the time of fragment formation). This suggests that the LEH at time of fragment formation is plausible for all energies.

F. Maxwellian distribution of velocities

In this section, we will show that the velocity distribution of the biggest source at time of fragment formation is indeed Maxwellian. Moreover, the temperature obtained from the standard deviation of the velocity distribution is almost exactly the same as that of Eq. (4), showing the consistency of our numerical studies. In Fig. 12, we show the histogram of the

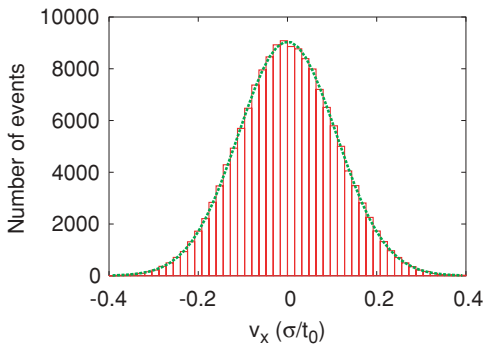

FIG. 12. (Color online) Velocity distribution (histogram) and Maxwellian fit (dotted line) for $E = +2.0\epsilon$.

TABLE I. Comparison of thermometers and statistical significance of the Maxwellian fit.

$E(\epsilon)$	$T_{\rm local}(\epsilon)$	$T_{\rm fit}(\epsilon)$	$T_{\rm event}(\epsilon)$	$T_{\rm shell}(\epsilon)$	S
−2.0	0.627 ± 0.043	0.623	0.645	0.647	0.86
0.0	0.619 ± 0.077	0.630	0.608	0.674	0.82
2.0	0.587 ± 0.062	0.575	0.506	0.558	0.78

velocity distribution at time of fragment formation and its Maxwellian fit for $E = 2.0\epsilon$.

In addition to observing the excellent agreement between the velocity distributions and their fits, we performed a Pearson χ^2 test, trying to reject the hypothesis that the distribution of velocities differs from that corresponding to the Maxwellian fit. We found a significance S above 0.25 for all cases, showing that even with a very low confidence level like CL = 0.80, we could reject the hypothesis that both distributions differ (i.e., the velocity distribution is indeed Maxwellian).

In Table I we show a cross comparison of different thermometers. To the results already presented, we add the temperature obtained from the Maxwellian fit of the velocity distribution, and we also show the obtained statistical significance.

G. Reducibility

Not long ago, Moretto and coworkers [23,24] proposed that the complex process of fragment emission could be described in terms of a binomial distribution. This approach rests on the assumption that a single transition probability p is capable of describing the emission process when no regard is paid to the mass or composition of the emitted fragments. In this way, the probability of emitting n fragments in a series of m trials

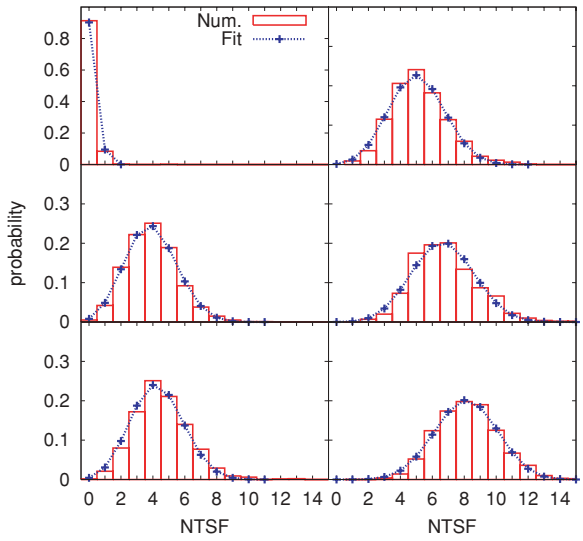

FIG. 13. (Color online) Probability distribution (histograms) and binomial fit (dotted line). For energies (from top to bottom and left to right): $E = -2.0\epsilon$, -0.2ϵ, 0.0ϵ, 0.2ϵ, 1.0ϵ, and 2.0ϵ.

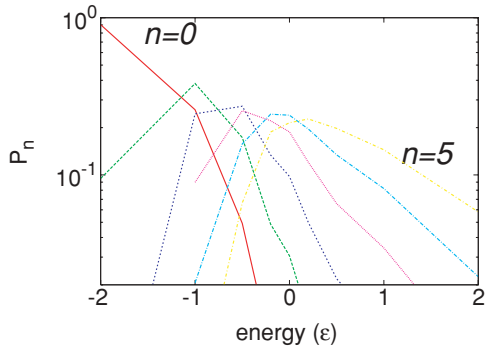

FIG. 14. (Color online) Probability of emiting 0 (red), 1 (green), 2 (blue), 3 (violet), 4 (cyan), and 5 (yellow) fragments as a function of energy.

should follow the well-known binomial distribution

$$P_n^m = \frac{m!}{n!(m-n)!} p^n (1-p)^{m-n}, \tag{11}$$

in which m stands for the number of "trials," while n stands for the number of successes. Following [23], we associate the parameter m with the maximum multiplicity for each energy and p with the transition probability. In Fig. 13, we show the result of such an analysis. The quality of the resulting fit is remarkable indeed, specially when one considers that we are facing an out-of-equilibrium nonsimultaneous process, while the very nature of the binomial process requires a constant value of p for the whole emission process.

To further illustrate the accuracy of this approach, we show in Fig. 14 the calculated probability of emitting n fragments during the entire process as a function of the total energy, with $n = 0$–5. P_n is calculated assuming a binomial distribution [Eq. (11)] with the value of p obtained from the best fit.

We will not further analyze the implications of this binomial fit because we have not yet been able to calculate microscopically the associated transitions barriers.

VI. CONCLUSIONS

In this paper, we have analyzed the dynamics and thermodynamics of fragment emission from excited sources interacting via a LJ potential. As this a classical system, our study provides only a framework for the analysis of fragmenting quantal systems. However, it gives relevant information since the LJ potential resembles the nuclear interaction force and is capable of undergoing phase transitions.

Focusing on the evolution of the biggest source and the corresponding emitted fragments, we have shown that the emission process cannot be cast into either a sequential or a simultaneous scenario, because even though there are many events in which fragments are emitted sequentially, the phenomenon of massive emission is frequent enough to forbid the characterization as a purely sequential one. Moreover, when looking at fragments well defined in configuration space, the process of emission cannot be cast into an isothermal one, i.e., temperatures are time dependent. Furthermore, there is a time dependence of the size of the emitting

source. Therefore, standard thermodynamical models that fix temperature and volume do not seem to be appropriate to revealing the true nature of the phenomenon under analysis. We have also shown, by analyzing the temperature of the source at the stage of most probable multiplicity, that it is possible to recover the caloric curve already obtained in the frame of phase-space analysis. If we recall Table I, we see that temperature can be determined according to a few reasonable definitions, which provide consistent results in all cases.

Two other interesting results have been obtained as a by product of these calculations. First, the velocity distribution functions of the particles that form the biggest source are strikingly Maxwellian for times larger than the time of fragment formation after the collective expanding mode is removed. Second, the probability of fragment emission (summed-up over all sizes) is remarkably binomial, suggesting a constancy of the transition amplitudes. We do not have a microscopic description of this constancy right now, but we are currently working on it.

We hope that these findings will encourage the development of new, more accurate and realistic models to describe nuclear multifragmentation.

ACKNOWLEDGMENTS

We acknowledge partial financial support from the University of Buenos Aires via Grant X308 and partial financial support from CONICET via Grant PIP 2304.

[1] J. Randrup and S. E. Koonin, Nucl. Phys. **A356**, 223 (1981).
[2] J. B. Bondorf, A. S. Botvina, A. S. Iljinov, I. N. Mishustin, and K. Sneppen, Phys. Rep. **257**, 133 (1995).
[3] G. Fai and J. Randrup, Nucl. Phys. **A381**, 557 (1982).
[4] C. B. Das, L. Shi, and S. Das Gupta, Phys. Rev. C **70**, 064610 (2004).
[5] J. M. Carmona, J. Richert, and P. Wagner, Eur. Phys. J. A **11**, 87 (2001).
[6] F. Gulminelli and P. Chomaz, Nucl. Phys. **A734**, 581 (2004).
[7] A. Strachan and C. O. Dorso, Phys. Rev. C **55**, 775 (1997).
[8] A. Strachan and C. O. Dorso, Phys. Rev. C **59**, 285 (1999).
[9] A. Chernomoretz, M. Ison, S. Ortiz, and C. O. Dorso, Phys. Rev. C **64**, 024606 (2001).
[10] X. Campi, H. Krivine, E. Plagnol, and N. Sator, Phys. Rev. C **67**, 044610 (2003).
[11] Y. Tosaka, A. Ono, and H. Horiuchi, Phys. Rev. C **60**, 064613 (1999) and references therein.
[12] J. Aichelin and H. Stocker, Phys. Lett. **B176**, 14 (1986).
[13] A. Chernomoretz, F. Gulminelli, M. J. Ison, and C. O. Dorso, Phys. Rev. C **69**, 034610 (2004).
[14] A. Strachan and C. O. Dorso, Phys. Rev. C **56**, 995 (1997).
[15] X. Campi and H. Krivine, Nucl. Phys. **A520**, 46 (1997).
[16] C. O. Dorso and J. Randrup, Phys. Lett. **B301**, 328 (1993).
[17] A. Strachan and C. O. Dorso, Phys. Rev. C **58**, R632 (1998).
[18] D. Kondepudi and I. Prigogine, *Modern Thermodynamics: From Heat Engines to Dissipative Structures* (Wiley, New York, 1998).
[19] W. Press, B. Flannery, S. Teukolsky, and W. T. Vetterling, *Numerical Recipes, The Art of Scientific Computing* (Cambridge University Press, Cambridge, 1989).
[20] A. Chernomoretz, P. Balenzuela, and C. O. Dorso, Nucl. Phys. **A723**, 229 (2003).
[21] P. Balenzuela, A. Chernomoretz, and C. O. Dorso, Phys. Rev. C **66**, 024613 (2002).
[22] J. B. Natowitz, R. Wada, K. Hagel, T. Keutgen, M. Murray, A. Makeev, L. Qin, P. Smith, and C. Hamilton, Phys. Rev. C **65**, 034618 (2002).
[23] L. G. Moretto, R. Ghetti, L. Phair, K. Tso, and G. J. Wozniak, Phys. Rep. **287**, 249 (1997).
[24] L. G. Moretto, L. Phair, K. Tso, and K. J. G. J. Wozniak, Nucl. Phys. **A583**, 513 (1995).